Optical and Electrical Properties of Three-Dimensional Interlinked Gold Nanoparticle Assemblies

Jurina M. Wessels,*,† Heinz-Georg Nothofer,† William E. Ford,†
Florian von Wrochem,† Frank Scholz,† Tobias Vossmeyer,† Andrea Schroedter,‡
Horst Weller,‡ and Akio Yasuda†

Contribution from Sony International (Europe) GmbH, Materials Science Laboratories, Hedelfingerstrasse 61, 70327 Stuttgart, Germany, and Institute of Physical Chemistry, University of Hamburg, Bundesstrasse 45, 20146 Hamburg, Germany

Received August 5, 2003; E-mail: wessels@sony.de

Abstract: The optical and electrical properties of 11–20 nm thick films composed of ∼4 nm gold nanoparticles (Au-NPs) interlinked by six organic dithiol or bis-dithiocarbamate derivatives were compared to investigate how these properties depend on the core of the linker molecule (benzene or cyclohexane) and its metal-binding substituents (thiol or dithiocarbamate). Films prepared with the thiol-terminated linker molecules, (1,4-bis(mercaptomethyl)benzene, 1,4-bis(mercaptomethyl)cyclohexane, 1,4-bis(mercaptoacetamido)benzene, and 1,4-bis(mercaptoacetamido)cyclohexane), exhibit thermally activated charge transport. The activation energies lie between 59 and 71 meV. These films show distinct plasmon absorption bands with maxima between 554 and 589 nm. In contrast, the film prepared with 1,4-cyclohexane-bis-(dithiocarbamate) has a significantly red-shifted plasmon band (∼626 nm) and a pronounced absorbance in the near infrared. The activation energy for charge transport is only 14 meV. These differences are explained in terms of the formation of a resonant state at the interface due to overlap of the molecular orbital and metal wave function, leading to an apparent increase in NP diameter. The film prepared with 1,4-phenylene-bis(dithiocarbamate) exhibits metallic properties, indicating the full extension of the electron wave function between interlinked NPs. In all cases, the replacement of the benzene ring with a cyclohexane ring in the center of the linker molecule leads to a 1 order of magnitude decrease in conductivity. A linear relationship is obtained when the logarithm of conductivity is plotted as a function of the number of nonconjugated bonds in the linker molecules. This suggests that nonresonant tunneling along the nonconjugated parts of the molecule governs the electron tunneling decay constant (β_{N-CON}), while the contribution from the conjugated parts of the molecule is weak (corresponding to resonant tunneling). The obtained value for β_{N-CON} is ∼1.0 (per non-conjugated bond) and independent of the nanoparticle-binding group. Hence, the molecules can be viewed as consisting of serial connections of electrically insulating (nonconjugated) and conductive (conjugated) parts.

Introduction

Two- and three-dimensional (3-d) assemblies of metal nanoparticles (NPs) exhibit interesting optical and electrical properties that are distinct from their respective bulk properties and can be designed on a molecular level. The characteristics of such semitransparent conductive films can be tuned by varying the size or shape of the particles as well as the distance between them. In addition, the electrical coupling between adjacent particles is controlled by the dielectric nature of the embedding organic matrix.[1–5] The high sensitivity of the electrical and optical properties of such assemblies toward their composition hence provides a unique possibility for optimizing the properties of these films for applications such as thin transparent conductive coatings, sensors,[6,7] or catalysis.[8]

The low-bias conductance of 3-d arrays of interlinked spherical Au-nanoparticle assemblies[2–5,7,9,10] and monolayer-protected Au-nanoparticle assemblies[1,6,8,11–13a] has been studied

---

† Sony International (Europe) GmbH.

‡ University of Hamburg.

(1) Terrill, R. H.; Potlethwaite, T. A.; Chen, C.-H.; Poon, C.-D.; Terzis, A.; Chen, A.; Hutchinson, J. E.; Clark, M. R.; Wignall, G.; Londono, J. D.; Superfine, R.; Falvo, M.; Johnson., C. S., Jr.; Samulski, E. T.; Murray, R. W. *J. Am. Chem. Soc.* **1995**, *117*, 12537.

(2) Musick, M. D.; Keating, C. D.; Keefe, M. H.; Natan, M. J. *Chem. Mater.* **1997**, *9*, 1499.

(3) Brust, M.; Bethell, D.; Shiffrin, D. J.; Kiely, C. J. *Adv. Mater.* **1995**, *7*, 795.

(4) Brust, M.; Bethell, D.; Kiely, C. J.; Schiffrin, D. J. *Langmuir* **1998**, *14*, 5425.

(5) Andres, R. P.; Bielefeld, J. D.; Henderson, J. I.; Janes, D. B.; Kolagunta, V. R.; Kubiak, C. P.; Mahony, W. J.; Osifchin, R. G. *Science* **1996**, *273*, 1690.

(6) Zamborini, F. P.; Leopold, M. C.; Hicks, J. F.; Kulesza, P. J.; Mali, M. A.; Murray, R. W. *J. Am. Chem. Soc.* **2002**, *124*, 8958.

(7) Vossmeyer, T.; Guse, B.; Besnard, I.; Bauer, R. E.; Muellen, K.; Yasuda, A. *Adv. Mater.* **2002**, *14*, 238.

(8) Musick, M. D.; Keating, C. D.; Lyon, L. A.; Botsko, S. L.; Pena, D. J.; Holliway, D.; McEvoy, T. M.; Richardson, J. N.; Natan, M. J. *Chem. Mater.* **2000**, *12*, 2869.

(9) Brust, M.; Kiely, C. J. *Colloids Surf. A* **2002**, *202*, 175.

(10) Joseph, Y.; Besnard, I.; Rosenberger, M.; Guse, B.; Nothofer, H.-G.; Wessels, J. M.; Wild, U.; Knop-Gericke, A.; Su, D.; Schlögl, R.; Yasuda, A.; Vossmeyer, T. *J. Phys. Chem.* **2003**, *107*, 7406.

in detail. Murray et al. used an Arrhenius-type activated tunneling model (eq 1) to describe the electron transport through a 3-d network of monolayer-protected gold nanoparticles:[13a]

$$\sigma_{EL}(\delta,T) = \sigma_0(e^{-\beta\delta})e^{-E_A/k_BT} \tag{1}$$

where β is the electron tunneling coefficient in units of Å^{-1}, δ the average interparticle distance,[13b] E_A the activation energy, and $\sigma_0 e^{-\beta\delta}$ the conductivity at $k_BT \gg E_A$. The first exponential term describes the electron tunneling between the particles through the organic matrix. Generally, the charge transport through molecules is governed by the nature of the molecule. Methylene (CH_2) groups are considered to be insulators. The Fermi level of the metal is located in the HOMO−LUMO gap of the molecule, and the side orbitals provide a superexchange pathway for the electrons to tunnel along the molecule. The conductivity depends exponentially on the length of the molecule. When the Fermi level of the metal becomes resonant or near resonant with the molecular orbital energy levels, the charge transport shows a weak length dependence.[14]

The second exponential term in eq 1 describes the activation energy for charge transport. Different models have been developed for theoretical description of the activation energy. On one hand, Abeles et al. developed a simple electrostatic model to describe the activation energy for the activated charge transport in granular metals. In the low-field regime, $\sigma \approx \exp[-2(C/RT)^{0.5}]$, where $C = \delta\beta E_{A,GM}$ and $E_{A,GM}$ corresponds to[15]

$$E_{A,GM} = \frac{e^2}{8\pi\epsilon\epsilon_0}\left(\frac{1}{r} - \frac{1}{r+\delta}\right) \tag{2}$$

where r is the radius of the particles, δ the interparticle distance, and ϵ the dielectric constant of the surrounding matrix. On the other hand, according to the Marcus theory, the free energy for activation (ΔG^*) of electron transfer can also be obtained from the repolarization of the organic dielectric matrix:

$$\Delta G^* = \frac{\lambda}{4} = \frac{e^2}{16\pi\epsilon_0}\left(\frac{1}{2r_1} + \frac{1}{2r_2} - \frac{1}{r}\right)\left(\frac{1}{\epsilon_{op}} - \frac{1}{\epsilon_s}\right) \tag{3}$$

where λ is the "outer sphere" reorganizational barrier energy, r_1 and r_2 are the radii of neighboring NPs, and r is the center−center distance between the NPs.[13] Murray and co-workers compared experimentally obtained activation energies from films of noninterlinked Au-NPs with both $E_{A,GM}$ and ΔG^*.[12,13] This comparison showed that neither of the models provides an adequate description of the experimentally observed activation energies.

It has been shown that an insulator−metal transition can be induced in 2-d and 3-d assemblies of metal NPs by changing the interparticle distance δ. Musick et al. observed an insulator−metal transition in 3-d films of 2-mercaptoethylamine interlinked

Au-NPs at sufficiently high surface coverage,[2,8] while Wohltjen and Snow showed that the transition in a film of monolayer-protected Au-NPs could be induced by varying the Au/alkanethiol capping molecule ratio due to alteration of the Au-NP diameter.[11] Brust et al. observed an insulator−metal transition in 3-d assemblies of 6 nm Au-NPs when the distance between the particles was reduced to ≤0.5 nm.[9] Heath and co-workers induced a reversible metal−insulator transition in a 2-d assembly of alkylthiol-stabilized Ag-NPs by reducing the interparticle spacing at the air/water interface on a Langmuir trough to values below $\delta/2r = 1.2$.[16]

Changes in the charge transport properties of self-assembled metal nanoparticle films are accompanied by changes in the optical absorption characteristics. In the insulating regime of 3-d networks of nanoparticles, an increase in conductivity is accompanied by a broadening and red-shift of the plasmon absorption band, as well as an increase in the absorption in the near infrared.[2,4,8−10] The absorption characteristics of colloidal Au-NPs, in solution and deposited on substrates, are determined by the local dielectric environment and size of the particles, the interparticle spacing,[17−21] and the chemical nature of the interface.[22,23] For isolated gold particles smaller than 25 nm, the extinction cross section of the collective electron resonance induced by the incident electromagnetic field is given by the dipole absorption:

$$\sigma_{abs}(\omega) = 9\frac{\omega}{c}V_0\epsilon_m^{3/2}\frac{\epsilon_2(\omega)}{[\epsilon_1(\omega) + 2\epsilon_m]^2 + \epsilon_2(\omega)^2} \tag{3}$$

where V_0 is the particle volume, ϵ_m is the dielectric constant of the surrounding medium, and $\epsilon(\omega) = \epsilon_1(\omega) + i\epsilon_2(\omega)$ is the dielectric constant of the particle. The peak position of the plasmon band is determined by the condition for resonance $\epsilon_1(\omega) = -2\epsilon_m$ and hence is governed by the dielectric function of the surrounding medium.[19] If the particles are closely packed, the average polarization field from the surrounding particles additionally influences the plasmon resonance.[18]

According to the chemical interface damping model developed by Persson, the shape and position of the plasmon band reflect not only the dielectric properties of the particles and the embedding matrix but also the nature of the chemical interface.[22,23] Static and dynamic charge transfer between adsorbate states and the particles can affect the phase coherence of the collective resonance. While the static charge transfer influences the electric double layer, the dynamic charge transfer influences the phase coherence of the conduction electrons. Dynamic charge transfer can take place when there is an overlap between the wave function of the metal nanoparticle and the molecular orbitals associated with the adsorbate, which leads to the formation of a resonant state. Electrons with energy levels close to the Fermi level or hot electrons can tunnel through the interface barrier into the resonant state and cause a dephasing of the plasmon oscillation.[22,23]

(11) Snow, A. W.; Wohltjen, H. *Chem. Mater.* **1998**, *10*, 947.
(12) Wuelfing, W. P.; Green, S. J.; Pietron, J. J.; Cliffel, D. E.; Murray, R. W. *J. Am. Chem. Soc.* **2000**, *122*, 11465.
(13) Wuelfing, W. P.; Murray, R. W. *J. Phys. Chem. B* **2002**, *106*, 3139. (b) Wuelfing, W. P.; Murray, *J. Phys. Chem. B* **2003**, *107*, 6018, Addition and Correction.
(14) Ratner, M. A.; Davis, B.; Kemp, M.; Mujica, V.; Roitberg, A.; Yaliraki, S. In *Molecular Electronics*; Avriam, A., Ratner, M., Eds.; Annals of the New York Academy of Science, Vol. 852; The New York Academy of Sciences: New York, 1998; p 22.
(15) Abeles, B.; Sheng, P.; Coutts, M. D.; Arie, Y. *Adv. Phys.* **1975**, *24*, 407.

(16) Markovich, G.; Collier, C. P.; Heath, J. R. *Phys. Rev. Lett.* **1998**, *80*, 3807.
(17) Underwood, S.; Mulvaney, P. *Langmuir* **1994**, *10*, 3427.
(18) Schmitt, J.; Mächtle, P.; Eck, D.; Möhwald, H.; Helm, C. A. *Langmuir* **1999**, *15*, 3526.
(19) Link, S. Mohamed, M. B.; El-Sayed, M. A. *Int. Rev. Phys. Chem.* **2000**, *19*, 409.
(20) Mulvaney, P. *Langmuir* **1996**, *12*, 788.
(21) Hövel, H.; Fritz, S.; Hilger, A.; Kreibig, U. *Phys. Rev. B* **1993**, *48*, 18178.
(22) Kreibig, U.; Gartz, M.; Hilger, A. *Ber. Bunsen-Ges. Phys. Chem.* **1997**, *101*, 1593.
(23) Persson, N. J. *Surf. Sci.* **1993**, *172*, 557.

This contribution for the first time introduces linker molecules that enable tuning of the conductivity in 3-d assemblies of Au-nanoparticles from the semiconducting to the metallic limit by varying the degree of conjugation of the linker molecule and the nature of its metal binding groups. We present results from optical and electrical characterizations of three-dimensional assemblies of Au-nanoparticles interlinked with novel dithiol- and dithiocarbamate derivatives as well as supporting results from TEM imaging and XRD measurements.

Experimental Section

Materials. All chemicals and solvents were reagent grade or higher quality and were used as received. Deionized water was purified using a Millipore Milli-Q system (18.2 MΩ cm). 1,4-Bis(mercaptomethyl)-benzene (BDMT) was purchased from Aldrich. The syntheses of 1,4-bis(mercaptoacetamido)cyclohexane (cHDMT), 1,4-bis(mercaptoacet-amido)benzene (DMAAB), 1,4-bis(mercaptoacetamido)cyclohexane (DMAAcH), disodium 1,4-cyclohexane-bis(dithiocarbamate) (cHBDT), and disodium 1,4-phenylene-bis(dithiocarbamate) (PBDT) are described in the Supporting Information. Dodecylamine-stabilized Au-NPs having a diameter of $d = 4.0 \pm 0.8$ nm were synthesized as described by Joseph et al.[10] Briefly, 160 mg of $AuCl_3$ was dissolved in 20 mL of H_2O. Tetraoctylammonium bromide (639 mg) in toluene (20 mL) was added. The mixture was vigorously stirred until the aqueous phase was colorless. Subsequently, dodecylamine (1.17 g) in toluene (20 mL) and a fresh solution of $NaBH_4$ (221 mg) in H_2O (15 mL) were added under vigorous stirring. The organic phase turned immediately from red-orange to deep purple. After stirring the mixture overnight two size selective precipitation steps were performed by adding each time 40 mL of ethanol to the organic phase and storing the solution overnight at -18 °C. The precipitates were separated by filtration through a nylon membrane (0.45 μm pore size) and redissolved in toluene. The second fraction was used for the preparation of the films.

Film Preparation. The interlinked Au-NP films were assembled onto BK7 glass substrates having lithographically defined interdigitated electrode structures with 20 μm gaps using the layer-by-layer assembly technique. The substrates were rinsed with acetone, hexane, and 2-propanol and then subjected to oxygen plasma treatment (Plasma PREP5, Gala Instruments, Germany). They were silanized by immersion into a solution of 50 μL of 3-aminopropyldimethylethoxysilane in 5 mL of toluene at 60 °C for 30 min. Subsequently, the silanized glass substrate was immersed for 15 min into a toluene solution of dodecylamine-stabilized Au-NPs whose concentration corresponded to an absorbance of 0.4 at $\lambda_{max} = 514$ nm (0.1 cm path length). After rinsing the substrate with toluene, it was exposed for 15 min to a 1 mM solution of the linker molecule and subsequently washed with the corresponding solvent of the linker molecule (toluene, DMF, or 2-propanol). The film growth was monitored by UV/vis spectroscopy. Successive exposures to the Au-NP and linker solutions were repeated until the maximum of the plasmon band reached an absorbance of ca. 0.3. During the assembly process the film grew on both sides of the glass substrate. Thus the actual film thickness corresponds to an absorbance of 0.15.

For XRD and TEM measurements, the films were prepared from nanoparticles interlinked in solution. The thoroughly washed precipitates were deposited onto Si substrates for XRD measurements and onto carbon grids (Plano) for TEM analysis. Drop casting was used for the preparation of the control sample of noninterlinked films of dodecyl-amine-stabilized Au-NPs.

Instruments. UV/vis absorption spectra were recorded using a Varian Cary 50 Scan spectrometer. Electrical characterization was performed using a home-built setup consisting of a liquid nitrogen container, a temperature control unit (Lake Shore), and a HP4241 source measure unit. The films were contacted using conductive Ag paint. The thickness of the assemblies was determined with a surface profiler (Tencor P10) along a scratch in the film. XRD measurements were performed with a Philips X'Pert PRO X-ray diffraction system, using the Cu Kα line ($\lambda = 154.06$ pm). TEM measurements were performed using the Tecnai F20 from FEI.
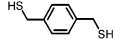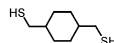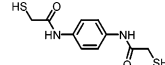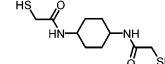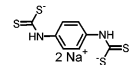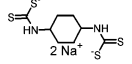
Results and Discussion

The molecules used for the assembly of the 3-d networks of interlinked Au-NPs can be grouped into three classes of molecules according to the substituents in the para positions of the benzene and cyclohexane cores. The molecules have either mercaptomethyl (BDMT, cHDMT), mercaptoacetamide (DMAAB, DMAAcH), or dithiocarbamate (PBDT, cHBDT) substituents for binding to gold. An overview of the linker molecules and the distances between opposing S atoms and S$^-$ atoms, respectively, as calculated by computational quantum chemistry software, is given in Table 1. The calculations were done with the program Dmol using density functional theory (DFT) at the nonlocal level. The Perdew–Wang generalized gradient-corrected functional (GGA)[24] was utilized together with a double numeric basis set with p- and d-polarized functions (DND).

Film Growth and Film Morphology. The films were prepared using the layer-by-layer assembly technique, and the growth of the films was monitored with UV/vis spectroscopy after the films reached a sufficient optical density, i.e., usually after the fifth deposition cycle. For all linker molecules the absorbance increases linearly with the number of deposition cycles, indicating that in each deposition cycle the same amount of material is deposited (Figure 1). However, the average slope of the curves varies slightly for the different linker molecules. The slope obtained from the films prepared with the bisdithio-carbamate linkers is roughly a factor of 1.8 smaller than the average slope obtained from the dithiol interlinked Au-NP films. The observed differences could be due to differences in the extinction coefficients of the NPs within the interlinked films, differences in the efficiency of exchanging the dodecylamine capping molecule with the linker molecule, or differences in packing density (vide infra).

Figure 2 shows TEM images of Au-NPs interlinked with DMAAcH (a), DMAAB (b), cHBDT (c), and PBDT (d), respectively. The networks of Au-NPs interlinked with DMAAcH and DMAAB are stable during TEM imaging. Both images (a and b in Figure 2) show well-isolated nanoparticles with particle to particle distances of roughly 1 nm. These values are slightly smaller than the S–S distance of the energy-minimized struc-tures of the linker molecules (Table 1). The networks of Au-NPs interlinked with cHBDT and PBDT are very sensitive to

(24) Perdew, J. P.; Chevary, J. A.; Vosko, S. H.; Jackson, K. A.; Pederson, M. R.; Singh, D. J.; Fiolhais, C. *Phys. Rev. B* **1992**, *46*, 6671.
(25) Link, S.; Mohamed, M. B.; El-Sayed, M. A. *J. Phys. Chem. B* **1999**, *103*, 3073.
(26) Chang, W.; Dong, S.; Wand, E. *Chem. Mater.* **2003**, *15*, 2495.
(27) Humeres, E.; Debacher, N. A.; Franco, J. D.; Lee. B. S.; Martendal, A. *J. Org. Chem.* **2000**, *67*, 3662.
(28) Humeres, E.; Debacher, N. A.; Sierra, M. M.de S. *J. Org. Chem.* **1999**, *64*, 1807.
(29) Wold, D. J.; Frisbie, C. D. *J. Am. Chem. Soc.* **2001**, *123*, 5549.
(30) The resistivity (ρ) of bulk gold at $T = 20$ °C is $\rho = 2 \times 10^{-8}$ Ω·m.
(31) Holmlin, R. E.; Ismagilov, R. F.; Haag, R.; Mujica, V.; Ratner, M. A.; Rampi, M. A.; Whitesides, G. M. *Angew. Chem. Int. Ed.* **2001**, *40*, 2316.
(32) Cui, X. D.; Zarate, X.; Tomfohr, J.; Sankey, O. F.; Primak, A.; Moore, A. L.; Moore, T. A.; Gust, D.; Harris, G.; Lindsay, S. M. *Nanotechnology* **2002**, *13*, 5.
(33) Anariba, F.; McCreery, R. L. *J. Phys. Chem. B* **2002**, *106*, 10355.
(34) Kornilovitch, P. E.; Bratkovsky, A. M.; Williams, R. S. *Phys. Rev. B* **2002**, *66*, 165436.

Table 1. Overview of Linker Molecules

Linker	Length (Å)	$\Delta(E_{HOMO-LUMO})$	
(1a) BDMT	7.7[a]	4.0	bis-mercaptomethylenes
(1b) cHDMT	8.2[a]	5.0	
(2a) DMAAB	14.8[a]	3.5	bis-acetamidothiols
(2b) DMAAcH	14.9[a]	4.7	
(3a) PBDT	10.7[b]	2.7	bis-dithiocarbamates
(3b) cHBDT	9.6[b]	3.2	

[a] S−S distance of energy-minimized structure. [b] S⁻−S⁻ distance of energy-minimized structure.
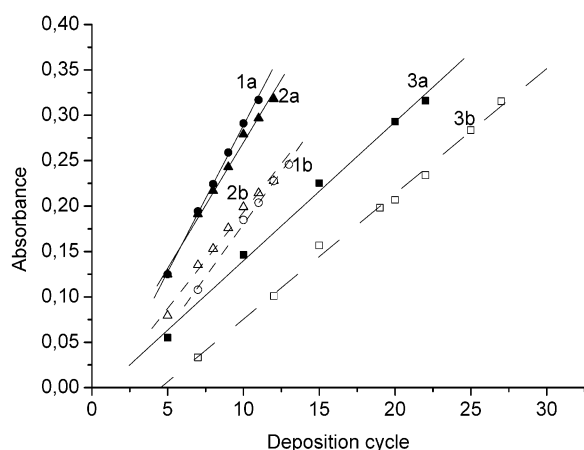
Figure 1. Absorbance of three-dimensional assemblies of Au-NPs interlinked with the bis-mercaptophenyl derivatives BDMT (**1a**) (●) and cHDMT (**1b**) (○), the bis-acetamidothiol derivatives DMAAB (**2a**) (▲) and DMAAcH (**2b**) (△), and the bis-dithiocarbamate derivatives PBDT (**3a**) (■) and cHBDT (**3b**) (□) plotted as a function of the deposition cycle after the fifth deposition cycle.

e-beam irradiation, causing rapid fusing of the Au-NPs upon irradiation. Results of such fusion processes are apparent in Figure 2c,d in several places. However, XRD measurements of Au-NPs interlinked with PBDT show that the half-width of the reflection size of the Au-NPs remains unchanged upon interlinking them with PBDT (Figure 3). The half-width of the (111) reflex corresponds to a particle diameter of 2.8 nm, which is slightly smaller than the particle diameter obtained from TEM (4.0 ± 0.8 nm). The slight difference between the average particle size obtained from TEM and the calculated particle size is probably due to lattice mismatches of the crystalline gold nanoparticles, which cause an additional broadening of the reflexes in the XRD measurements. The grain boundaries of the particles, however, remain stable after cross-linking with PBDT, indicating that the observed changes in particle diameter during TEM imaging are solely induced by e-beam irradiation. At locations where fusion processes did not take place, well-separated NPs were observed in several TEM images (e.g., Figure 2c and d), showing interparticle distances of roughly 1 nm for cHBDT and PBDT. On the basis of these results, we

assume that the Au-NP packing density is comparable for the films interlinked with DMAAB, DMAAcH, cHBDT, and PBDT.

Optical Properties. Figure 4 shows characteristic absorption spectra of the three-dimensional assemblies of Au-NPs interlinked by the three classes of molecules. The Au-NP films interlinked with the dithiols BDMT, cHDMT, DMAAB, and DMAAcH exhibit a distinct plasmon band between 550 and 590 nm and have a blue-red appearance. In contrast the Au-NP film interlinked with cHBDT has a blue-green appearance and a significantly broadened plasmon band. The film prepared with PBDT appears to be greener compared to the film prepared with cHBDT. In addition it exhibits also some golden color in reflection. The film displays absorption characteristics similar to bulk gold.

The plasmon band maxima of the Au-NP films interlinked with BDMT and DMAAB are red-shifted in comparison to the maxima of the Au-NP films interlinked with cHDMT and DMAAcH, respectively (Table 2). These values are reproducible within an uncertainty of ca. ±4 nm. In case of the mercapto-methylene linker molecules, exchanging the cyclohexane core with a benzene core causes a red shift in the plasmon band of ∼31 nm. The difference in the S−S distance is 0.5 Å. In the case of the acetamidothiols the shift is only ∼19 nm. The differences in the S−S length is 0.1 Å. These results indicate that the observed shifts in the peak position of the plasmon band are not solely determined by changes in the length of the linker molecule but that the polarizability of the linker molecule largely contributes to the observed shifts.[17,18,20,21]

Within this context, it is further interesting to note that for both types of linker molecules the films prepared with the cyclohexane derivatives are ∼5 nm thicker (see Table 2) than the films prepared with the benzene derivatives, although the films have the same absorbance. This is due to differences in the number of assembly cycles necessary to reach an optical density of 0.3 in the plasmon band maximum (Figure 1). If the number of assembly cycles is kept constant, the absorbance of the film varies between the cyclohexane and benzene derivatives accordingly. It has been shown, in agreement with the Mie theory, that with increasing dielectric constant the plasmon resonance shifts to the red and the intensity of the plasmon band
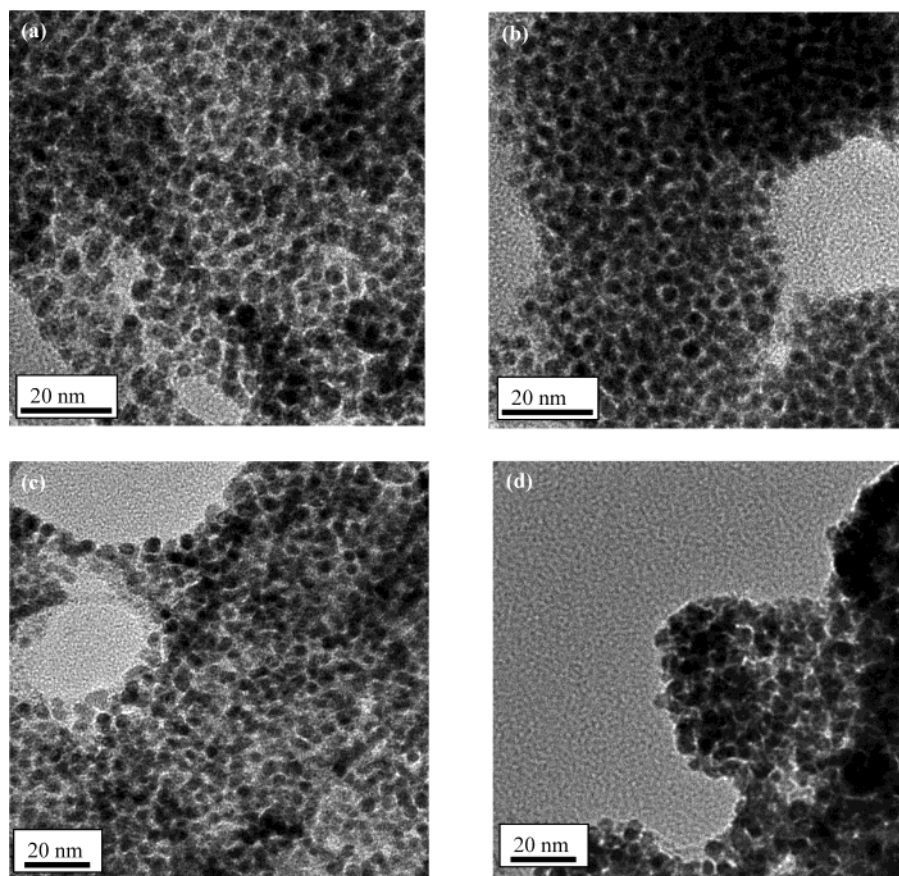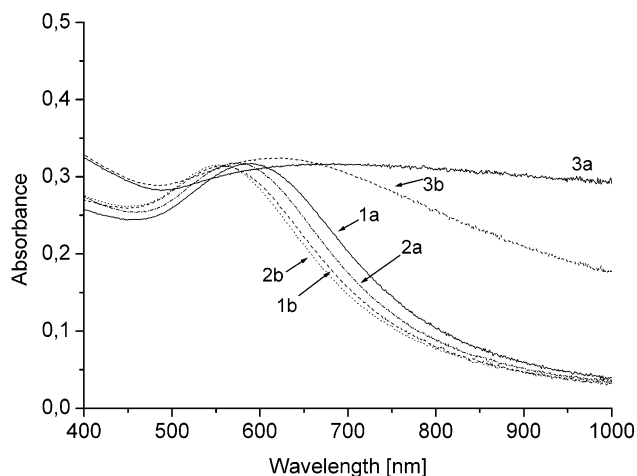
Figure 2. TEM images of Au-NPs interlinked with the acetamidothiol derivatives DMAAcH (a) and DMAAB (b) and with the bis-dithiocarbamate derivatives cHBDT (c) and PBDT (d).
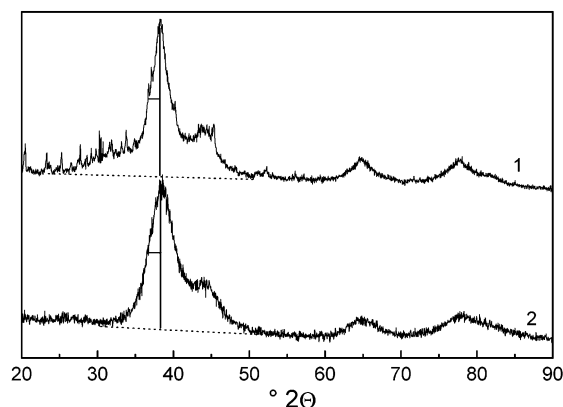
Figure 3. XRD spectra of a film of Au-NPs interlinked in solution with the bis-dithiocarbamate PBDT (1) and of a film of noninterlinked dodecylamine-stabilized Au-NPs (2) prepared by drop casting (control). The small scattering signals are probably due to PBDT crystals that formed upon drying of the film from excess of the linker molecule.

Figure 4. Absorption spectra of three-dimensional assemblies of Au-NPs interlinked with the bis-mercaptomethylene derivatives BDMT (**1a**) and cHDMT (**1b**), the bis-acetamidothiol derivatives DMAAB (**2a**) and DMAAcH (**2b**), and the bis-dithiocarbamate derivatives PBDT (**3a**) and cHBDT (**3b**).

increases.[17,18,20,25,26] This indicates that the extinction cross section is smaller for the films interlinked with the cyclohexane derivatives than for the films interlinked with the benzene derivatives.

More pronounced changes are apparent in the absorption spectra of the bis-dithiocarbamate (PBDT, cHBDT) interlinked Au-NP assemblies (Table 2). In the case of PBDT (**3a**), the plasmon band is nearly absent and the film exhibits a strong absorbance in the near infrared, similar to the absorption spectra of gold films. A distinct broadening of the plasmon band and increase in absorbance in the near-IR is also observed with

cHBDT (**3b**); however, the spectrum still exhibits a distinct plasmon band maximum at 626 nm. The peak position is reproducible with an uncertainty of ca. ±20 nm. As noted earlier, metallic absorption spectra have been observed previously for Au-NP assemblies containing short thiols or dithiols. The absorption spectrum of PBDT (**3a**) (Figure 4) is comparable to the absorption spectrum of a film of 6 nm sized Au-NPs interlinked with propanedithiol, where the spectral changes were attributed to the close proximity of the nanoparticles.[9] For films

Table 2. Overview of the Film Characteristics

| linker	d (nm)[a]	λ_{max} (nm)	E_A (meV)	resistivity (Ωm)
(**1a**) BDMT	13.5	589	59.7	0.09
(**1b**) cHDMT	19.8	558	58.8	0.85
(**2a**) DMAAB	13.4	573	65	4.2
(**2b**) DMAAcH	18.1	554	71	92.8
(**3a**) PBDT	11.1			0.0008
(**3b**) cHBDT	12.3	626	13.8	0.0042

[a] Film thickness d.

of Au-NPs interlinked with 2-mercaptoethylamine, Natan and co-workers observed with increasing surface coverage a transition from a spectrum exhibiting a plasmon band to a spectrum displaying the characteristics of bulk gold.[2,8] In the present case, however, the distinct broadening of the plasmon band as well as the metallic absorption characteristics seem to be specific to the nature of the dithiocarbamate linker molecules, since they are evident from the start of the assembly process (see Supporting Information). In addition, the results obtained from the TEM images provide support that the interparticle separation is approximately 1 nm and determined by the length of the linker molecule (vide supra).

Kreibig et al. observed for metal clusters embedded in various dielectric metal oxides a distinct red-shift and broadening of the plasmon band with increasing dielectric constant of the embedding matrix.[22] These plasmon band characteristics were explained in terms of the chemical interface-damping model.[23] Excited electrons that are transferred between adsorbate induced resonant states and the metal NPs disturb the phase coherence of the surface plasmon as a result of inelastic scattering processes and hence lead to a broadening of the plasmon band. This requires an overlap between molecular orbital and metal wave functions,[23] which creates a resonant state close to the Fermi level of the metal-NPs. It is described in the literature that the strong electron-withdrawing nature of the thiocarbonyl introduces a pronounced double bond characteristic to the C−N bond in the bis-dithiocarbamate moiety and inhibits the delocalization of the nitrogen electron pair into the benzene ring.[27,28] The electron-withdrawing nature of the thiocarbonyl may also influence the electron distribution in the Au−S bond. It is anticipated that the conjugated nature of the dithiocarbamate group, which is directly coupled to the Au-NPs, leads to the formation of a resonant state, causing the pronounced changes in the absorption characteristics of the films.

Electronic Transport Properties. The current−voltage measurements show ohmic behavior for all films between ±1 V in the temperature range between 100 and 300 K. The resistivities of the films at 295 K are summarized in Table 2. The experimental uncertainty obtained from three to five different assemblies is approximately ±10%. For all three classes of molecules, the resistivity of the film increases by roughly 1 order of magnitude when the benzene ring is substituted with a cyclohexane ring. The same order of magnitude difference in the resistivity was observed in metal−molecule−metal tunnel junctions fabricated from benzyl thiol SAMs and hexyl thiol SAMs (vide infra).[29]

The conductivity is plotted as a function of T^{-1} in Figure 5. Except for the film of PBDT interlinked Au-NPs, which displays metallic behavior, the films exhibit transport characteristics of a percolated network of nanoparticles; that is, the conductivity decreases with decreasing temperature. The electron transport
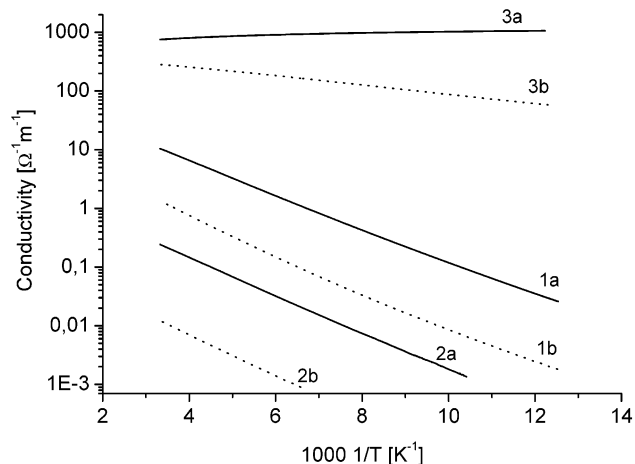
Figure 5. $\sigma(T)$ characteristics of three-dimensional assemblies of Au-NPs interlinked with the bis-mercaptomethyl derivatives BDMT (**1a**), cHDMT (**1b**), the bis-acetamidothiol derivatives DMAAB (**2a**), DMAAcH (**2b**), and the bis-dithiocarbamate derivatives PBDT (**3a**) and cHBDT (**3b**).

in such films can be described in terms of a thermally activated tunneling process between particles.[10,13] From the slope of the curves we obtained the activation energy E_A for charge transport (Table 2). The activation energies of the BDMT and cHDMT interlinked films ($E_A \approx 58-59$ meV) and DMAAB and DMAAcH interlinked films ($E_A \approx 65-71$ meV) are, within the experimental uncertainty of ca. ±10%, similar in value and lie in the range reported for self-assembled films of Au-NPs interlinked by alkanedithiols using also dodecylamine-stabilized Au-NPs prepared according to the same protocol ($d = 4.0 ± 0.8$ nm).[10]

The distinct differences in the absorption characteristics of the dithiol and dithiocarbamate interlinked Au-NP films are also apparent in the electrical characteristics of the assemblies. The film of PBDT interlinked Au-NPs shows metallic behavior; that is, the conductivity increases with decreasing temperature. This is in agreement with the optical properties of this film displaying absorption characteristics of bulk metal (vide supra). Metallic charge transport characteristics have been previously observed in propanedithiol interlinked Au-NP films.[9] Natan and co-workers observed insulator−metal transitions for films consisting of ∼6 nm Au-NPs interlinked by 2-mercaptoethylamine at sufficient high surface coverage, as mentioned above.[2] This transition was attributed to the close proximity of the nanoparticles and a resulting overlap of the wave function from the nanoparticles. In the PBDT interlinked Au-NP film, however, the distance between the nanoparticles is roughly twice as large compared to the 2-mercaptoethylamine interlinked films. The above-described results indicate that, due to the high degree of conjugation of PBDT and the good Au-NP/molecule contact, the electron wave function between neighboring NPs also overlaps. Metallic properties were also observed for ∼150 nm thick films of 11 nm Au-NPs capped with 2-mercaptoethanol. The resistivity of these films was $5 × 10^{-6}$ Ω·m, which is only 200 times that of bulk gold.[2,8] The resistivity of the $13.8 ± 2.1$ nm thick PBDT interlinked Au-NP film at 295 K is $8 × 10^{-4}$ Ω·m, which is about 3−4 orders of magnitude above that of bulk gold.[30] Since the conductivity in such films is roughly proportional to the third power of the NP diameter (for NPs having diameters comparable or smaller than the de Broglie
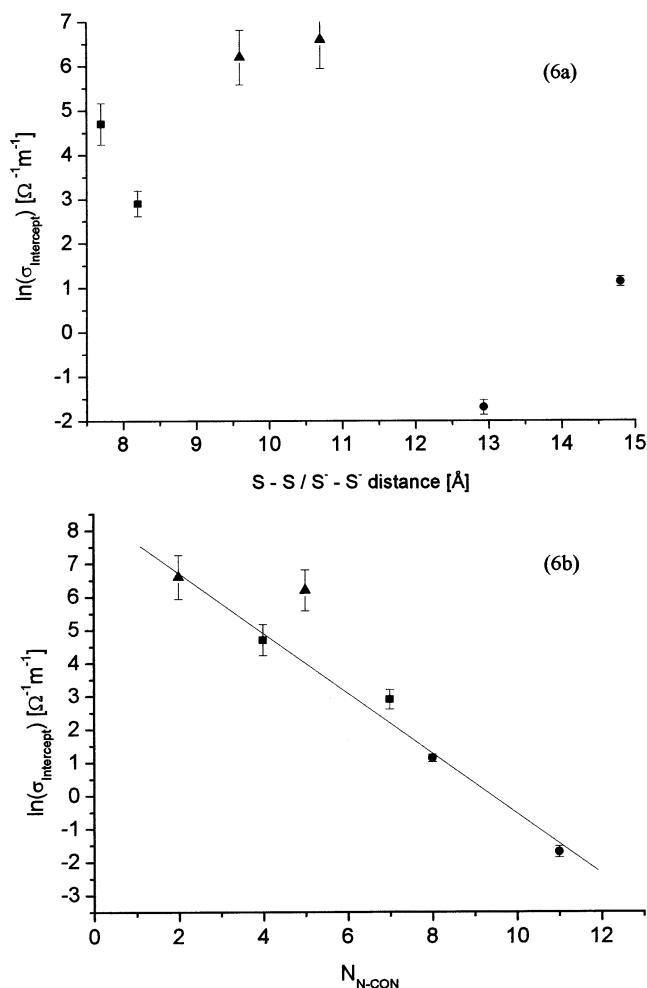
Figure 6. (a) Plot of $\ln(\sigma_{Intercept})$ as a function of the length of the linker molecule. The length of the bis-mercaptomethylene (■) and bis-acetamidothiol (●) and bis-dithiocarbamate (▲) linker molecules corresponds to the S—S and S⁻—S⁻ distances of the energy-minimized structures. (b) Plot of $\ln(\sigma_{Intercept})$ as a function of the number of nonconjugated bonds in the bis-mercaptomethylene (■) and bis-acetamidothiol (●), and bis-dithiocarbamate (▲) linker molecules, where the dithiocarbamate group is considered to be conjugated.

wavelength),[11] these differences in conductivity can be mainly attributed to differences in the diameter of the Au-NPs.

The activation energy for the cHBDT interlinked Au-NP film (E_A = 13.8 meV) is ∼4–5 times smaller than the activation energies obtained from the films assembled with the dithiol derivatives. As described above, the optical characteristics of the films indicate that the strong electron-withdrawing nature of the thiocarbonyl group leads to an overlap of the molecular orbital and metal wave function that could lead to an apparent increase in the Au-NP diameter. On the basis of the granular metal theory,[15] an effective increase in particle radius of 2.4 Å, which corresponds to the Au—S bond distance in a thiocarbamate/Au conjugate, should lead to a decrease in the activation energy of a factor of ∼3.

Equation 1 predicts a linear relationship between $\ln(\sigma)$ and the interparticle distance δ. By extrapolating the plots in Figure 5, we obtain the intercept $\ln(\sigma_{Intercept}) = [\ln(\sigma_0) - \beta\delta]$. In Figure 6a, $\ln(\sigma_{Intercept})$ is plotted as a function of the S—S distance in case of the dithiols and the S⁻—S⁻ distance in case of the bis-dithiocarbamates, respectively. The error bars reflect the measurement uncertainty in the conductivity of the 3-d films

as obtained from three to five different films for each linker molecule. There is no evidence for a clear linear relationship between $\ln(\sigma_{Intercept})$ and the distance between the nanoparticles, as it has been previously observed for NP films comprised of alkanethiol-stabilized Au-NPs[1,13] and metal–molecule–metal junctions.[29,31,32] Similar scattering in plots of $\ln(\sigma_{Intercept})$ vs δ was also observed by Murray and co-workers for thin films of arenethiol monolayer-protected Au clusters.[13] They obtained a clear linear relationship when $\ln(\sigma_{Intercept})$ was plotted as a function of the number of methylene units, however. Taking into consideration the conjugated nature of the C—N bond in the dithiocarbamate moiety (vide supra), we find a linear relationship between $\ln(\sigma_{Intercept})$ and the number of nonconjugated bonds (N_{N-CON}) (Figure 6b), suggesting that $\sigma \approx \sigma_0 \exp(-\beta_N N_{N-CON})$. This indicates that electron tunneling through the conjugated parts of the molecules does not contribute significantly to the decay of the electron wave function. For resonant tunneling processes, only a weak dependence of the electron transmission on the number of conjugated bonds is expected.[33] Thus, these data suggest that the electron transport through these molecules is partially nonresonant along the side orbitals and partially resonant through the conjugated parts of the molecule. In other words, the molecules can be viewed as consisting of two electrically insulating (the nonconjugated) parts in series with conductive (conjugated) parts. This is in agreement with the theoretical description of rectifying asymmetric molecules by Williams and co-workers, where a conducting level such as a benzene ring is placed asymmetrically between insulating alkane chains.[34] From Figure 6b it is evident that the $\ln(\sigma_{Intercept})$ values obtained for cHDMT and cHBDT deviate from the linear fit. This may be due to the fact that all single bonds were treated as being equivalent, with respect to their electronic coupling.

From the slope of the linear fit (Figure 6b) we obtain $\beta = 0.99$ per N_{N-CON}, which is comparable to the values reported for noninterlinked alkanethiol-stabilized Au-NP films[13] and SAMs of alkanethiols[29,31,32] but larger than the values obtained from alkanedithiol interlinked Au-NP films ($0.61 \le \beta \le 0.71$)[10] and alkanedithiol SAMs contacted at both ends ($\beta = 0.57$).[35] The smaller values of β in the latter two cases were attributed to the fact that the molecules were contacted at both ends. Recently, however, Xu and Tao reported a tunneling decay constant of $\beta = 1.0 \pm 0.1$ for *n*-alkanedithiols.[36] The results described above suggest that the contact to the nanoparticles through either thiol or thiocarbamate groups is not the determining factor for β, since the data obtained from the respective linker molecules fall on the same line. Whether the lower β-value obtained from films of alkanedithiol interlinked Au-NPs is related to the flexibility of the linker molecules and associated changes in the geometry of the films or to the fact that our linker molecules contain different heteroatoms needs to be resolved in further experiments.

In this context it is further pertinent to note that, within each class of linker molecules, the Au-NP films interlinked with the benzene derivatives are 1 order of magnitude more conductive than the films interlinked with the cyclohexane derivatives (vide supra). Wold and Frisbie observed this difference also between

(35) Cui, X. D.; Primak, A.; Zarate, X.; Tomfohr, J.; Sankey, O. F.; Moore, A. L.; Moore, T. A.; Gust, D.; Nagahara, L. A.; Lindsay, S. M. *J. Phys. Chem. B* **2002**, *106*, 8609.
(36) Xu, B.; Tao, N. J. *Science* **2003**, *301*, 1221.

benzyl thiol SAMs and to hexyl thiol SAMs and attributed this change in the resistance to differences in the HOMO−LUMO gap between phenyl rings ($\Delta E_{\text{HOMO}-\text{LUMO}} \approx 4$ eV) and alkyl chains ($\Delta E_{\text{HOMO}-\text{LUMO}} \approx 8$ eV).[29] When comparing the difference in the HOMO−LUMO gap of the bis-mercaptomethyl, bis-mercaptoacetamido, and bis-dithiocarabamate derivatives, there is no clear relationship between these and the electrical properties of the films (Table 1). However, 1 order of magnitude difference in the conductivity of alkanedithiol interlinked Au-NP films is also observed upon increasing the number of methylene units by three. This corresponds to the number of additional nonconjugated bonds in the cyclohexane-based linker molecules, if all single bonds can be treated as being equivalent.[9,10]

The conductivity of the film prepared with cHBDT is 1 order of magnitude larger than the film prepared with BDMT, despite the fact that the interparticle distance is larger and the linker molecule has five nonconjugated bonds (PBDT has only four nonconjugated bonds). We note, however, that the activation energy is roughly a factor of 4 smaller in the case of cHBDT. According to eq 1, a factor of ~4 difference in E_A would lead to 1 order of magnitude difference in conductivity if the number of nonconjugated bonds is constant. Taking into consideration the difference in the number of nonconjugated bonds between cHDMT and BDMT, the observed difference in E_A would lead to roughly a factor of 4 difference in the conductivity.

In summary, these investigations on a variety of novel dithiol and bis-dithiocarbamate linker molecules show that the metal/molecule contact has a pronounced influence on the optical and electrical properties of the films. The nonresonant tunneling process along the nonconjugated parts of a molecule mainly determines the electron tunneling decay constant, while the contribution from the conjugated parts is negligible, corresponding to a resonant tunneling through the conjugated parts of the molecule. These effects make it possible to tune the conductivity from the insulating to the metallic limit without altering significantly the interparticle spacing.

Supporting Information Available: Synthesis and analytical characterization of Au-NPs and linker molecules, additional absorption spectra of Au-NP films interlinked with PBDT and cHBDT. This material is available free of charge via the Internet at http://pubs.acs.org.

JA0377605